International Journal of Heat and Mass Transfer 53 (2010) 376–383

Contents lists available at ScienceDirect

International Journal of Heat and Mass Transfer

journal homepage: www.elsevier.com/locate/ijhmt

# An investigation of the thermal performance of cylindrical heat pipes using nanofluids

Maryam Shafahi [a], Vincenzo Bianco [b], Kambiz Vafai [a,*], Oronzio Manca [b]

[a] Department of Mechanical Engineering, University of California Riverside, Riverside, CA 92521, USA
[b] Dipartimento di Ingegneria Aerospaziale e Meccanica, Seconda Università degli Studi di Napoli, Via Roma 29, 81031 Aversa (CE), Italy

ARTICLE INFO

*Article history:*
Received 28 July 2009
Received in revised form 30 August 2009
Accepted 30 August 2009
Available online 23 October 2009

*Keywords:*
Heat pipe
Thermal performance
Nanofluids

ABSTRACT

In this work, a two-dimensional analysis is used to study the thermal performance of a cylindrical heat pipe utilizing nanofluids. Three of the most common nanoparticles, namely $Al_2O_3$, CuO, and $TiO_2$ are considered as the working fluid. A substantial change in the heat pipe thermal resistance, temperature distribution, and maximum capillary heat transfer of the heat pipe is observed when using a nanofluid. The nanoparticles within the liquid enhance the thermal performance of the heat pipe by reducing the thermal resistance while enhancing the maximum heat load it can carry. The existence of an optimum mass concentration for nanoparticles in maximizing the heat transfer limit is established. The effect of particle size on the thermal performance of the heat pipe is also investigated. It is found that smaller particles have a more pronounced effect on the temperature gradient along the heat pipe.



## 1. Introduction

Heat pipes and their applications in thermal management have been studied for decades. They constitute an efficient, compact tool to dissipate substantial amount of heat from various engineering systems including electronic components. Heat pipes are able to dissipate substantial amount of heat with a relatively small temperature drop along the heat pipe while providing a self-pumping ability due to an embedded porous material in their structure. A limiting factor for the heat transfer capability of a heat pipe is related to the working fluid transport properties. In order to overcome this limitation, the thermophysical properties of the fluid can be improved. An innovative way to enhance liquid thermal conductivity is the dispersion of highly conductive solid nanoparticles within the base fluid. This new generation of conductive fluids with nanoparticles are referred to as nanofluids [1]. The nanoparticles within the fluid change the other thermophysical properties such as density and viscosity. A number of investigations have been conducted to study boiling and natural and forced convection using nanofluids [2].

Due to the useful features of a nanofluid, various research groups [3–14] have tried to engage it within a heat pipe and study the subsequent thermal enhancement experimentally. Different nanoparticles such as silver [3,8,11,13], CuO [5,9], diamond [6,12], titanium [4,7], nickel oxide [10], and gold [14] have been utilized within the heat pipe working fluid. The improved thermal performance is observed through a reduction in thermal resistance [3,6–9,11,13,14], a drop in the temperature gradient along the heat pipe [3,12,13], an increase in the heat pipe efficiency [4], and an enhancement in the overall heat transfer coefficient [10]. In some studies [5,9], the existence of an optimum amount of nanoparticle mass concentration providing the highest thermal performance has been established. Liu et al. [9] have shown that the heat pipe operating pressure has a significant effect on the thermal performance. In another study, Riehl [10] has observed that a higher heat transfer coefficient can be seen when using nanoparticles in water under low heat input conditions. Tsaia [14] investigated the influence of particle size on the heat pipe thermal performance.

Almost all of the research work on the use of nanoparticles in heat pipes is experimental. To the best of authors' knowledge; there is a lack of information in modeling heat pipe characteristics in the presence of a nanofluid. The focus of the present work is to model the influence of a nanofluid on the thermal performance of a heat pipe. A comprehensive analytical model proposed by Zhu and Vafai [15] is modified to include the effects of nanofluids within a cylindrical heat pipe. A common range of concentration for different nanoparticles, namely $Al_2O_3$, CuO, and $TiO_2$ in water is considered as the operational fluid within the heat pipe under various heat inputs. The temperature profile, thermal resistance, and the maximum heat transfer limits are investigated. A significantly higher thermal performance is observed due to a reduction in the thermal resistance as well as the end to end temperature gradient. Furthermore, the maximum capillary limit heat transfer increases when using a nanofluid as the working fluid. To the best of our knowledge, there is no study on the effect of a nanofluid on the

* Corresponding author. Tel.: +1 951 827 2135; fax: +1 951 827 2899.
*E-mail address:* vafai@engr.ucr.edu (K. Vafai).

0017-9310/$ - see front matter © 2009 Elsevier Ltd. All rights reserved.
doi:10.1016/j.ijheatmasstransfer.2009.09.019

**Nomenclature**

| | |
|---|---|
| $K$ | permeability of the wick [$m^2$] |
| $k$ | thermal conductivity [W/m K] |
| $k_{eff}$ | effective thermal conductivity of the liquid-saturated wick [W/m K] |
| $k_{layer}$ | nanolayer thermal conductivity [W/m K] |
| $k_{wall}$ | thermal conductivity of the heat pipe wall [W/m K] |
| $h$ | convective heat transfer coefficient [$W/m^2$ K] |
| $h_{fg}$ | latent heat of the working fluid [KJ/Kg] |
| $L$ | length of the heat pipe [m] |
| $L_a$ | length of the adiabatic section [m] |
| $L_c$ | length of the condenser section [m] |
| $L_e$ | length of the evaporator section [m] |
| $P$ | Pressure [Pa] |
| $Q$ | input heat [W] |
| $Q_c$ | heat transfer rate at the condenser section [W] |
| $Q_e$ | heat transfer rate at the evaporator section [W] |
| $r$ | cylindrical coordinates [m] |
| $r_p$ | nanoparticles radius [nm] |
| $r_c$ | effective pore radius of the wick [m] |
| $R_o$ | heat pipe's outer radius [m] |
| $R_t$ | heat pipe thermal resistance [K/W] |
| $R_v$ | vapor core radius [m] |
| $R_w$ | heat pipe's inner radius [m] |
| $T$ | temperature [K] |
| $T_b$ | bulk temperature of the coolant in cooling jack [K] |
| $u$ | horizontal velocity component [m/s] |
| $U$ | velocity along the axis [m/s] |
| $v$ | vertical velocity component [m/s] |
| $v_1$ | vapor injection velocity [m/s] |
| $v_2$ | vapor suction velocity [m/s] |
| $w$ | nanolayer thickness [nm] |
| $x$ | cylindrical coordinates [m] |

*Greek symbols*

| | |
|---|---|
| $\phi$ | particle concentration |
| $\varepsilon$ | porosity of the wick |
| $\gamma$ | porous wick shape parameter $\left(\sqrt{\varepsilon/K}\right)$ |
| $\mu$ | dynamic viscosity [N s/$m^2$] |
| $\mu^+$ | dimensionless dynamic viscosity $\left(\frac{\mu_l}{\mu_v}\right)$ |
| $\rho$ | density [$kg/m^3$] |
| $\rho^+$ | dimensionless density $\left(\frac{\rho_l}{\rho_v}\right)$ |
| $\sigma_l$ | surface tension of the working fluid [N/m] |

*Subscripts*

| | |
|---|---|
| 0 | heat pipe with pure fluid |
| *bf* | base fluid |
| *i* | liquid–vapor interface |
| *l* | liquid phase |
| max | maximum |
| *nf* | nanofluid |
| *np* | nanoparticle |
| *p* | particle |
| *v* | vapor |

*Superscript*

| | |
|---|---|
| + | dimensionless quantity |

maximum heat transfer in heat pipes. Our results establish the existence of an optimum concentration of nanoparticles within the working fluid with respect to attaining the maximum heat transfer. This optimum concentration is established for different nanofluids under different operational conditions.

## 2. Analysis

The schematic of a cylindrical heat pipe used in the present analysis is given in Fig. 1.

Heat applied at the evaporator section causes vaporization and, consequently, a pressure increase in the working fluid. The vapor formed in the evaporator flows towards the condenser as a result of the pressure difference between the evaporator and condenser regions. Vapor condenses releasing its latent heat in the condenser and the condensate flows back to the evaporator through the porous wick thus completing the cycle. The mathematical model adopted in this work is based on the following assumptions: the process is steady state; radiative and gravitational effects are negligible and the fluid is considered Newtonian and incompressible.

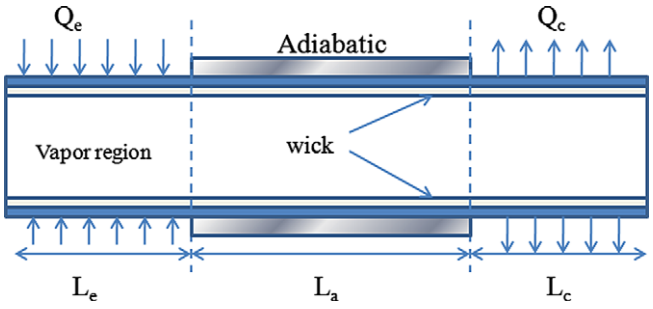


**Fig. 1.** Schematic of a cylindrical heat pipe under consideration.

Moreover, the injection and suction velocities at the liquid–vapor interface are considered to be uniform. Also, the wick is assumed to be isotropic and saturated with the working fluid. The liquid flow within the porous wick is modeled using the generalized momentum equation [16].

### 2.1. Governing equations

The mass and momentum conservation equations for liquid and vapor regions are [15]:

*Vapor region*

$$\frac{\partial u_v}{\partial x}+\frac{\partial v_v}{\partial r}+\frac{v_v}{r}=0 \tag{1}$$

$$\rho_v\left(u_v\frac{\partial u_v}{\partial x}+\frac{\partial u_v}{\partial r}\right)=-\frac{\partial p_v}{\partial x}+\mu_v\left(\frac{\partial^2 u_v}{\partial r^2}+\frac{1}{r}\frac{\partial u_v}{\partial r}\right) \tag{2}$$

$$\frac{\partial p_v}{\partial r}=0 \tag{3}$$

*Liquid region*

$$\frac{\partial u_l}{\partial x}+\frac{1}{r}\frac{\partial}{\partial r}(ru_l)=0 \tag{4}$$

$$\frac{\mu_l}{\varepsilon}\left(\frac{\partial^2 u_l}{\partial r^2}+\frac{1}{r}\frac{\partial u_l}{\partial r}\right)-\frac{\mu_l}{K}u_l-\frac{\rho_l F\varepsilon}{K^{1/2}}|u_l|u_l-\frac{\partial p_l}{\partial x}=0 \tag{5}$$

where $\varepsilon$, $K$, and $F$, are porosity, permeability and a geometric function based on the porous wick structure described in Vafai [17].

### 2.2. Analytical solution

The analysis of Zhu and Vafai [15] is modified to incorporate the presence of a nanofluid within the heat pipe. The analysis is carried

on to obtain the velocity, pressure, temperature, and the maximum heat transfer limit for the heat pipe for various operational conditions using nanofluids.

### 2.2.1. Liquid velocity profile

The maximum liquid velocity profile is determined by integrating the liquid continuity and applying proper boundary conditions [15]. The liquid velocity can be presented as:

$$U_l(x)=\begin{cases}-Bv_1x & 0\le x\le L_e\\ -Bv_1L_e & L_e\le x\le L_e+L_a\\ -Bv_2(L-x) & L_e+L_a\le x\le L_e+L_a+L_c\end{cases}\qquad L=L_e+L_a+L_c \tag{6}$$

where $B$ is given in Table 1 and can be seen that it is dependent on the liquid density.

### 2.2.2. Liquid and vapor pressure distributions

Liquid and vapor pressure distributions are obtained by integrating the momentum equations in the radial direction. Applying the appropriate boundary conditions [15]; the pressure distributions can be presented as:

*Vapor pressure*

$$p_v(x)=p_v(0)+\begin{cases}\left(Gv_1^2+Mv_1\right)x^2 & 0\le x\le L_e\\ \left(Gv_1^2-Mv_1\right)L_e^2+2Mv_1L_ex & L_e\le x\le L_e+L_a\\ \left(Gv_2^2-Mv_2\right)(x-L)^2+Mv_2(L+L_a)L_c & L_e+L_a\le x\le L_e+L_a+L_c\end{cases} \tag{7}$$

*Liquid pressure*

$$p_l(x)=p_l(0)+\begin{cases}G_2v_1x^2 & 0\le x\le L_e\\ G_2v_1L_e(2x-L_e) & L_e\le x\le L_e+L_a\\ -G_2v_2[(x-L)^2-(L+L_a)L_c] & L_e+L_a\le x\le L_e+L_a+L_c\end{cases} \tag{8}$$

where $v_1$ and $v_2$ are vapor injection and suction velocities and $G$, $M$, and $G_2$ are given in Table 1. It can be seen that the liquid pressure explicitly depends on the density and viscosity of the working fluid. Nanofluid's density is calculated based on a simple representation of the particle and fluid phases which has been shown to provide a reasonable result based on the experimental work of Pak and Cho [20], while a classical model proposed by Brinkman [21] is used to obtain the viscosity. As such the density and viscosity of the nanofluid can be presented as:

$$\rho_{nf}=\rho_p\phi+(1-\phi)\rho_{bf} \tag{9}$$

$$\mu_{nf}=\frac{\mu_{bf}}{(1-\phi)^{2.5}} \tag{10}$$

### 2.2.3. Temperature distribution

The wall temperature profile is obtained assuming uniform wall temperature along the condenser and evaporator sections. A heat conduction model is used for the wall and liquid-wick region. As such, the heat pipe temperature profile can be presented in the following form [15]:

$$T_{wall}(x)=\begin{cases}T_b+\frac{Q}{2\pi L_c}\left[\left(\frac{\ln\left(\frac{R_o}{R_w}\right)}{k_{wall}}+\frac{\ln\left(\frac{R_w}{R_p}\right)}{k_{eff}}\right)\left(1+\frac{L_c}{L_e}\right)+\frac{1}{hR_o}\right] & 0\le x\le L_e\\ T_b+\frac{Q}{2\pi L_c}\left(\frac{\ln\left(\frac{R_o}{R_w}\right)}{k_{wall}}+\frac{\ln\left(\frac{R_w}{R_p}\right)}{k_{eff}}+\frac{1}{hR_o}\right) & L_e\le x\le L_e+L_a\\ T_b+\frac{Q}{2\pi L_chR_o} & L_e+L_a\le x\le L\end{cases} \tag{11}$$

where $k_{wall}$ is the thermal conductivity of the heat pipe wall and $k_{eff}$ is the effective thermal conductivity of the liquid-saturated wick. The steady state operation in the condenser can be presented as:

$$Q_c=2\pi R_oL_ch(T_{wall,c}-T_b) \tag{12}$$

where $R_o$, $L_c$, $h$, $T_{wall,c}$, and $T_b$ are the heat pipe's outer radius, length of the condenser section, outside convective heat transfer coefficient, wall temperature at the condenser section and the bulk temperature of the coolant.

Temperature distribution results are compared with the experimental results of Huang et al. [22] and were found to be in very good agreement. It can be seen that the heat pipe performance is closely linked to the employed working fluid properties. Particularly, the temperature distribution is dependent on the effective thermal conductivity of the porous wick which can be presented as [18]:

$$k_{eff}=\frac{k_{nf}[(k_{nf}+k_s)-(1-\varepsilon)(k_{nf}-k_s)]}{[(k_{nf}+k_s)+(1-\varepsilon)(k_{nf}-k_s)]} \tag{13}$$

As seen in Eq. (13), $k_{eff}$ is a function of nanofluid and solid matrix conductivities and porosity of the wick. Using a nanofluid within the heat pipe improves its thermal performance primarily through an increase in the thermal conductivity of the working fluid. $k_{eff}$ increases when thermal conductivity of the nanofluid, $k_{nf}$, is increased and it leads to an enhancement of the thermal performance of the heat pipe. Nanofluid's thermal conductivity is obtained using the model proposed by Yu and Choi [19,23] which can be presented as:

**Table 1**
Analytical solution parameters.

| | |
|---|---|
| $A=\frac{(G_2-2M_1)(L+L_a)}{4\pi R_v\rho_vh_{fg}}$ | $B=\frac{2R_v}{\rho_{nf}^+(R_w^2-R_v^2)}\left(1+\frac{8\rho^+}{\mu^+\gamma^2R_v^2}\right)$ |
| $C=\frac{8}{\mu_{nf}^+\gamma R_v^2}-B$ | $D=CR_v$ |
| $G_2=\frac{\mu_{nf}}{2K}\left(B+\frac{1}{\gamma R_v}\frac{2C}{1-\left(\frac{R_w}{R_v}\right)^2}\right)$ | $M=-\frac{4\mu_v}{R_v^2}(D-2)$ |
| | $G=-\frac{\rho_v}{3R_v^2}(D^2-7D+16)$ |

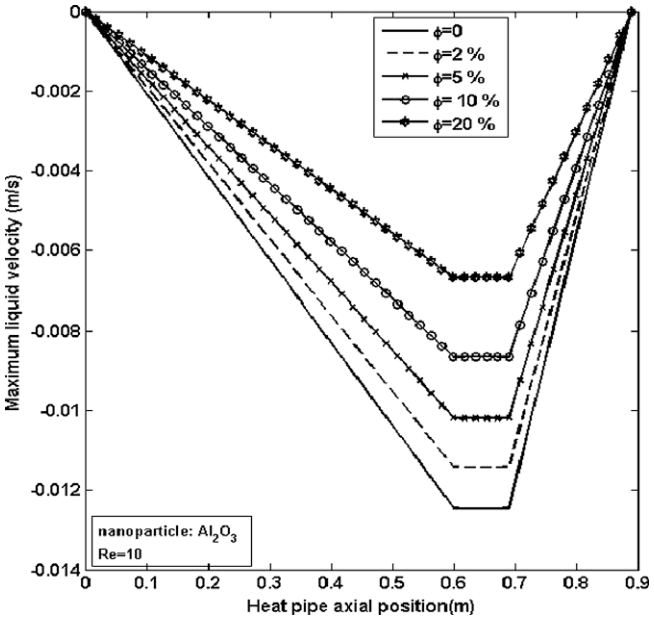


**Fig. 2.** The effect of nanoparticle concentration levels on the maximum liquid velocity profile.

$$k_{nf} = \frac{k_{pe} + 2k_l + 2(k_{pe} - k_l)(1+\beta)^3\phi}{k_{pe} + 2k_l - (k_{pe} - k_l)(1+\beta)^3\phi} k_l \tag{14}$$

$$k_{pe} = \frac{[2(1-\alpha) + (1+\beta)^3(1+2\alpha)]\alpha}{-(1-\alpha) + (1+\beta)^3(1+2\alpha)} k_p \tag{14a}$$

$$\alpha = \frac{k_{layer}}{k_p}; \quad \beta = \frac{w}{r_p} \tag{14b}$$

where $k_p$ and $k_{layer}$ are the thermal conductivities of the nanoparticle and nanolayer, respectively. They proposed a modified Maxwell model to account for the effect of the nanolayer, by replacing the thermal conductivity of solid particles in the Maxwell model with the modified thermal conductivity of particles $k_{pe}$ as seen in Eq. (14a). A nanoparticle with the radius $r_p$ is assumed to be surrounded by a nanolayer of thickness w. This model has the advantage of linking the nanofluid's thermal conductivity to the nanoparticle's diameter; taking into account the effect of diameter variation on the thermal behavior of the fluid. The base fluid physical properties change vs temperature, is taken into account for the applied range of 297 K < $T$ < 370 K.

*2.2.4. Maximum heat transfer limit*

The capillary pressure of the wick provides a steady state operational pressure for the heat pipe. The maximum heat input that a heat pipe can remove can be obtained based on the capillary pressure limit as:

$$\Delta p_v(x_{\max} - x_{\min}) + \Delta p_l(x_{\max} - x_{\min}) + p_c(x_{\min}) = \frac{2\sigma_l}{r_c} \tag{15}$$

To solve Eq. (15); it is necessary to know vapor and liquid pressure distributions, which are obtained by integrating the vapor and liquid momentum equations in the radial direction. The maximum heat transport by the heat pipe when boundary and inertial effects are neglected can be presented as [15]:

$$Q_{\max} = \frac{2\sigma_1}{Ar_c} \tag{16}$$

The maximum heat transport capillary limit is affected by the density and viscosity of the nanofluid as seen in Eqs. (15) and (16) and Table 1.

## 3. Results and discussion

The analysis was carried out by incorporating the effect of nanofluids in the analytical model given by Zhu and Vafai [15]. The heat pipe considered in the present paper has a total length of 89 cm. The condenser has a length of 20 cm, while the evaporator and adiabatic sections are 60 and 9 cm in length, respectively. The outer radius of the heat pipe is taken as 9.55 mm, the inner radius is 9.4 mm and the vapor core radius is 8.65 mm. It should be noted that the dimensions used here are just nominal. We have established that the presented results hold for a substantial variation in the nominal geometrical dimensions given in here.

In the present analysis, three different types of water based nanofluids, namely $Al_2O_3$, CuO, and $TiO_2$ were considered. In this work, a reasonable concentration range is chosen for different particle sizes and the performance of the cylindrical heat pipe is investigated for different heat inputs. In what follows, the influence of nanofluid on liquid velocity, pressure profile, temperature profile, thermal resistance, and maximum heat transport capability is investigated.

As seen in Fig. 2, the maximum liquid velocity decreases when increasing the nanoparticle concentration within the working fluid. This is due to an increase in the liquid density in the presence of more nanoparticles, as can be seen in Eq. (9). As a result of this increase in the nanofluid density, a slower liquid flow is observed. Fig. 3 displays the effect of nanoparticles on liquid and vapor pressure distributions. With respect to the liquid pressure, it can be seen that initially the pressure gradient decreases as the concentration of the nanoparticles increases. This trend continues up to a specific concentration of nanoparticles within the working fluid. However, this trend reverses once the concentration increases beyond this specific value. It is observed that pressure distribution along the heat pipe changes slightly between 5% and 10% of nanofluid concentration and there is a reversal effect on the pressure distribution changes when the concentration reaches 20%. This behavior is due to the opposite roles played by density and viscosity, both growing with particle concentration in the liquid. At the beginning, density effect prevails leading to a smaller pressure drop. After reaching a critical concentration level, the increase in viscosity overcomes the density effect resulting in a larger liquid

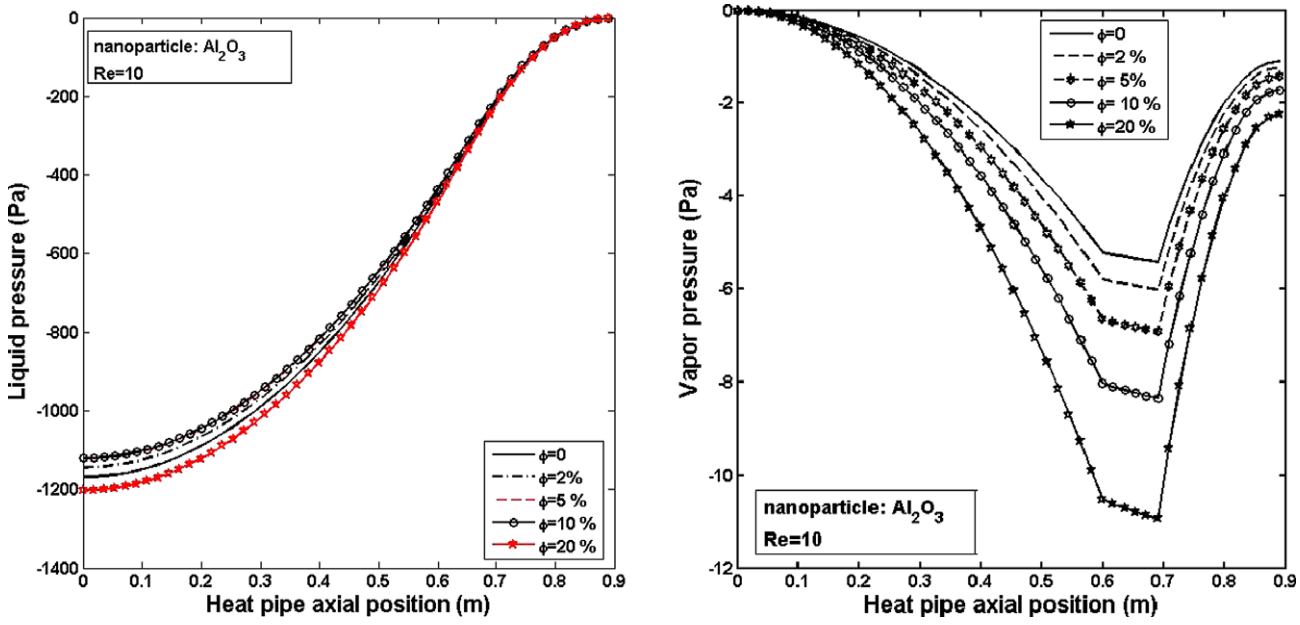


**Fig. 3.** The effect of nanoparticle concentration levels on the liquid and vapor pressure distributions.

pressure drop. Physically, an increase in density reduces the liquid velocity which in turn results in a lower shear stress. In contrast, an increase in viscosity increases the shear stress. These two opposite effects cause the presence of a critical concentration for nanoparticles. Fig. 3 also shows that the vapor pressure drop increases when particle concentration increases. This is due to the changes in the physical properties of vapor and liquid as seen in Eq. (7) and Table 1. Fig. 4 shows the wall temperature distribution for different nanofluids with different concentration levels. The figure clearly highlights the positive impact of the nanoparticles on the thermal performance of the heat pipe. A lower temperature difference between evaporator and condenser can be observed when nanofluids are used. For a 4% particle concentration, the temperature gradient is reduced by 5%, 3%, and 5% for $Al_2O_3$, TiO2, and CuO, respectively.

The effect of particle diameter and concentration levels on the temperature difference between evaporator and condenser for various heat loads is shown in Fig. 5. The figure shows that increasing the particle concentration decreases the temperature difference between the evaporator and condenser. Moreover, the temperature difference decreases with a reduction in particle diameter. It can be seen that for a constant temperature difference between condenser and evaporator the use of a nanofluid as the working fluid allows the heat pipe to operate under a larger heat load. A nanofluid based heat pipe is able to dissipate up to 26% more heat without experiencing an increase in the wall temperature.

Fig. 6 shows that it is possible to down size a heat pipe's dimension when using nanofluid as the working fluid. In this figure, $L_0$ is the nominal length of a water based heat pipe and $L$ designates the length for the nanofluid based heat pipe. As can be seen in Fig. 6, there is a significant reduction in the size of a heat pipe when using a nanofluid. For example, the presence of 10 nm CuO particles in water results in 78% reduction in the nominal size.

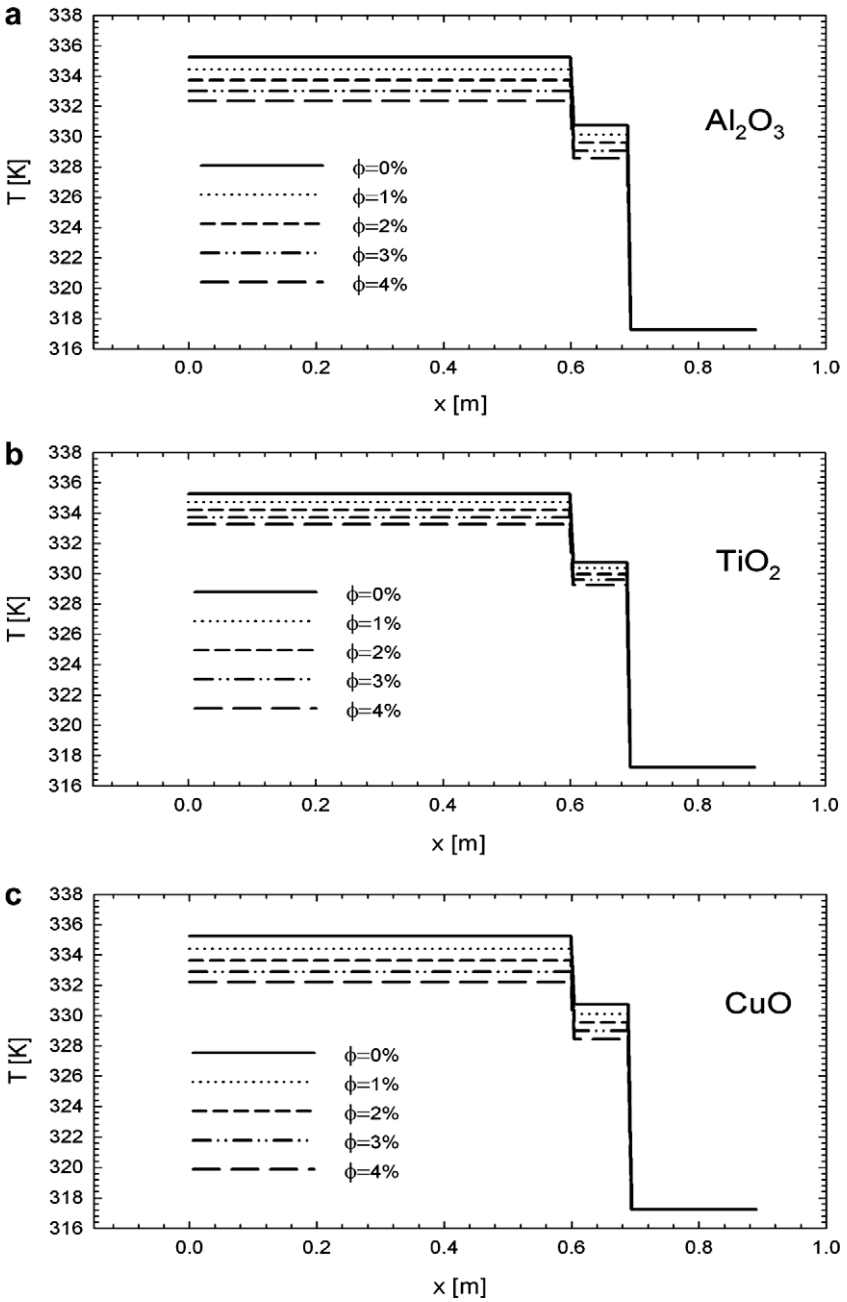


**Fig. 4.** Heat pipe temperature distribution for different particle concentration levels analyzing different nanoparticles (a) $Al_2O_3$, (b) $TiO_2$, and (c) CuO; $d_p = 20$ nm.

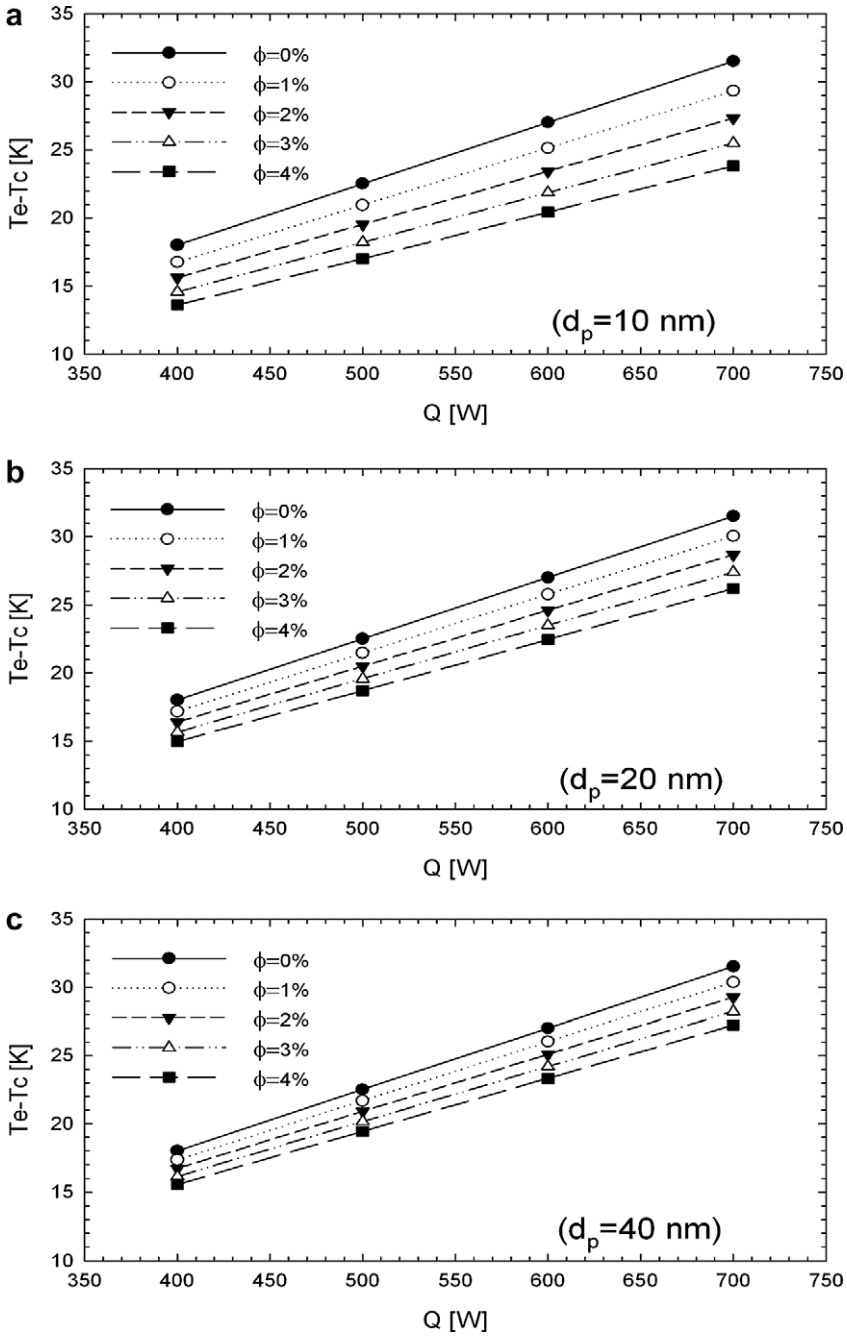


**Fig. 5.** Effect of CuO particle concentration levels on the thermal performance of a heat pipe under various heat input and for different particle diameters: (a) $d_p$ = 10 nm, (b) $d_p$ = 20 nm, and (c) $d_p$ = 40 nm.

The influence of different nanoparticle concentration levels on the heat pipe thermal resistance is shown in Fig. 7. The thermal resistance of the heat pipe is defined as

$$[Q/(T_e - T_c)]^{-1}.$$

In this figure, the thermal resistance ratio of the heat pipe with nanofluid over one with pure water is shown. A nominal particle diameter of 10 nm is utilized and the heat load is varied from 200 to 800 W. It can be seen that increasing the nanoparticle concentration decreases the heat pipe thermal resistance and provides a better performance. For example, a 75% reduction in the thermal resistance ratio is obtained for a 4% CuO nanoparticle concentration level.

Fig. 8 represents the maximum heat transport capillary limit as function of particles concentration for all the investigated nanofluids. Fig. 8 clearly establishes the existence of an optimum nanoparticle concentration level for each nanofluid in maximizing the thermal performance of the heat pipe. Increasing the nanoparticle concentration enhances the maximum heat transfer until a critical concentration level is reached. After this critical level, an increase in the concentration decreases the maximum heat transfer. It is worth mentioning that both density and viscosity changes have a substantial effect on the thermal performance of the heat pipe. This is similar to what was experienced with the liquid pressure and once again is due to the opposite roles that density and viscosity have in affecting the $Q_{max}$. From a physical point of view, this

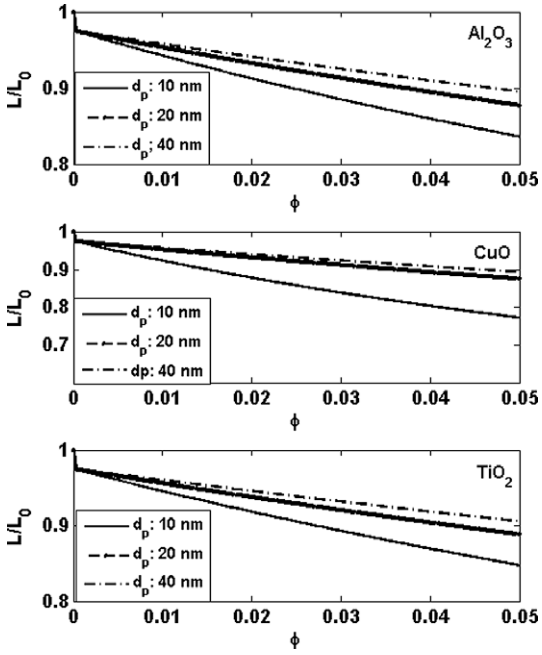


**Fig. 6.** Effect of different particle diameter and concentration levels on the size of the heat pipe (a) $Al_2O_3$, (b) $TiO_2$, and (c) CuO. ($T_{wall} \leqslant 90$ °C).

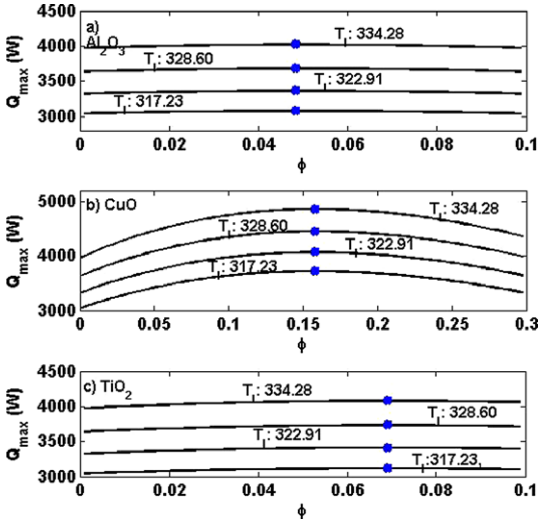


**Fig. 8.** The effect of nanoparticles concentration levels on the maximum heat load carrying capability of the heat pipe for different condenser temperatures, (a) $Al_2O_3$; (b) CuO; (c) $TiO_2$.

occurs due to an increase in density and viscosity with an increase in the concentration level which results in a larger mass flow and higher pressure loss, respectively. These two factors have positive and negative effects on $Q_{max}$, resulting in the existence of an optimum particle concentration level. As seen in Fig. 8, the optimum concentration for $Al_2O_3$, CuO, and $TiO_2$ are about 5%, 15%, and 7%, respectively.

The effect of porous media characteristics, shown in terms of $\gamma$, on the maximum heat transfer can be seen in Figs. 9 and 10. Fig. 9 represents the $Q_{max}$ variations vs changes in nanoparticle concentration level and $\gamma$. The smaller $\gamma$ corresponds to the larger permeability of the porous wick and bigger maximum heat load of the heat pipe.

Fig. 10 shows the effect of variation in $\gamma$ on the $Q_{max}$. It can be seen that increasing $\gamma$ reduces the maximum heat load capacity of the heat pipe. The three dimensional representation for the maximum heat transfer in terms of nanoparticle concentration and $\gamma$ is shown in Fig. 10. The existence of an optimum value of nanoparticle concentration level in maximizing the heat load capacity can be seen in this figure.

## 4. Conclusions

The thermal performance of cylindrical heat pipes utilizing a nanofluid as the working fluid has been investigated. Three of the most common nanoparticles, namely $Al_2O_3$, CuO, and $TiO_2$ are considered. The heat pipe velocity, pressure, temperature, and maximum heat transfer limit are obtained for different nanoparticle concentration levels and sizes. Moreover, the possibility of reducing the size of the cylindrical heat pipe by utilizing nanofluids

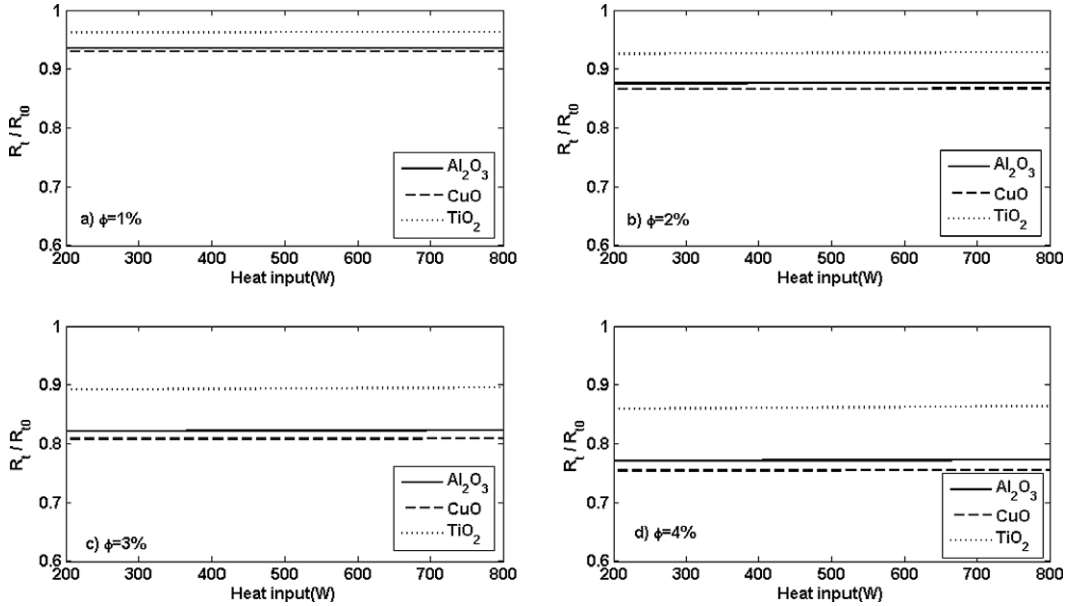


**Fig. 7.** The effect of different nanoparticle concentration levels on the heat pipe thermal resistance. (a) $\phi = 1\%$; (b) $\phi = 2\%$; (c) $\phi = 3\%$; (d) $\phi = 4\%$.

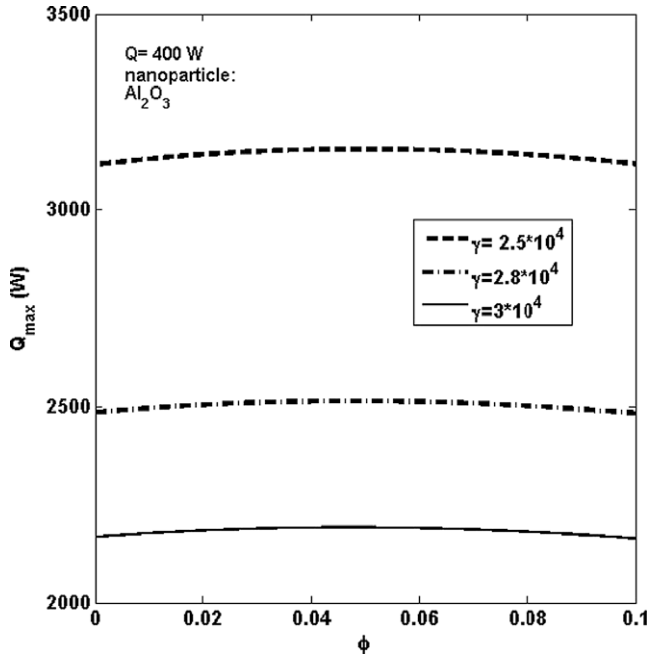


**Fig. 9.** The effect of porous media shape parameters ($\gamma$) and nanoparticle concentration levels on the maximum heat transfer capability of the heat pipe.

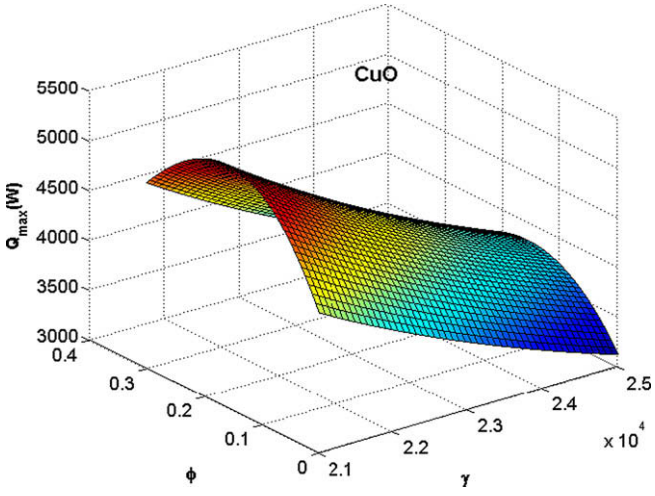


**Fig. 10.** Surface representation of the heat pipe maximum heat transfer in terms of nanoparticle concentration level and the porous media shape parameters ($\gamma$).

is studied. The results from our model confirm previous experimental results, i.e., the thermal performance of a heat pipe is improved and temperature gradient along the heat pipe and thermal resistance across the heat pipe are reduced when nanofluids are utilized as the working fluid. It is shown that the thermal resistance decreases as the concentration increases or as the particle diameter decreases. The influence of nanofluid and the geometrical characteristics of the wick on the maximum heat load carrying capability of the cylindrical heat pipe is investigated. The existence of an optimum concentration level in producing the maximum heat transfer is established.

## References

[1] S.U.S. Choi, Enhancing thermal conductivity of fluids with nanoparticles, ASME FED 231 (1995) 99–105.
[2] S. Kakac, A. Pramuanjaroenkij, Review of convective heat transfer enhancement with nanofluids, Int. J. Heat Mass Transfer 52 (2009) 3187–3196.
[3] S.W. Kang, W.C. Wei, S.H. Tsai, S.Y. Yang, Experimental investigation of silver nano-fluid on heat pipe thermal performance, Appl. Therm. Eng. 26 (2006) 2377–2382.
[4] P. Naphon, D. Thongkum, P. Assadamongkol, Heat pipe efficiency enhancement with refrigerant–nanoparticles mixtures, Energy Convers. Manage. 50 (2009) 772–776.
[5] X.F. Yang, Z.H. Liu, J. Zhao, Heat transfer performance of a horizontal micro-grooved heat pipe using CuO nanofluid, J. Micromech. Microeng. 18 (2008) 035038.
[6] H.B. Ma, C. Wilson, Q. Yu, K. Park, U.S. Choi, M. Tirumala, An experimental investigation of heat transport capability in a nanofluid oscillating heat pipe, J. Heat Transfer 128 (2006) 1213–1216.
[7] P. Naphon, P. Assadamongkol, T. Borirak, Experimental investigation of titanium nanofluids on the heat pipe thermal efficiency, Int. Commun. Heat Mass Transfer 35 (2008) 1316–1319.
[8] S.W. Kang, W.C. Wei, S.H. Tsai, C.C. Huang, Experimental investigation of nanofluids on sintered heat pipe thermal performance, Appl. Therm. Eng. 29 (2009) 973–979.
[9] Z. Liu, J. Xiong, R. Bao, Boiling heat transfer characteristics of nanofluids in a flat heat pipe evaporator with micro-grooved heating surface, Int. J. Multiphase Flow 33 (2007) 1284–1295.
[10] R.R. Riehl, Analysis of loop heat pipe behavior using nanofluid, in: Heat Powered Cycles International Conference (HPC), New Castle, UK, Paper 06102, 2006.
[11] Y. Chen, W. Wei, S. Kang, C. Yu, Effect of nanofluid on flat heat pipe thermal performance, in: 24th IEEE SEMI-THERM Symposium, pp. 16–19.
[12] H.B. Ma, C. Wilson, B. Borgmeyer, K. Park, Q. Yu, S.U.S. Choi, M. Tirumala, Effect of nanofluid on the heat transport capability in an oscillating heat pipe, Appl. Phys. Lett. 88 (2006) 143116.
[13] Y. Lin, S. Kang, H. Chen, Effect of silver nano-fluid on pulsating heat pipe thermal performance, Appl. Therm. Eng. 28 (2008) 1312–1317.
[14] C.Y. Tsaia, H.T. Chiena, P.P. Dingb, B. Chanc, T.Y. Luhd, P.H. Chena, Effect of structural character of gold nanoparticles in nanofluid on heat pipe thermal performance, Mater. Lett. 58 (2004) 1461–1465.
[15] N. Zhu, K. Vafai, Analysis of cylindrical heat pipes incorporating the effects of liquid–vapor coupling and non-Darcian transport – a closed form solution, Int. J. Heat Mass Transfer 42 (1999) 3405–3418.
[16] K. Vafai, C.L. Tien, Boundary and inertia effects on flow and heat transfer in porous media, Int. J. Heat Mass Transfer 24 (1981) 195–203.
[17] K. Vafai, Convective flow and heat transfer in variable porosity media, J. Fluid Mech. 147 (1984) 233–259.
[18] S.W. Chi, Heat Pipe Theory and Practice, Hemisphere, Washington, DC, 1976.
[19] S.K. Das, S.U.S. Choi, W. Yu, T. Pradeep, Nanofluids Science and Technology, John Wiley & Sons, Hoboken, 2008.
[20] B.C. Pak, Y.I. Cho, Hydrodynamic and heat transfer study of dispersed fluids with submicron metallic oxide particles, Exp. Heat Transfer 11 (1998) 151–170.
[21] H.C. Brinkman, The viscosity of concentrated suspensions and solution, J. Chem. Phys. 20 (1952) 571–581.
[22] L. Huang, M.S. El-Genk, J.-M. Tournier, Transient performance of an inclined water heat pipe with a screen wick, in: ASME National Heat Transfer Conference, Atlanta, Heat Pipes and Capillary Pumped Loops, vol. 236, 1993, pp. 87–92.
[23] W. Yu, S.U.S. Choi, The role of interfacial layers in the enhanced thermal conductivity of nanofluids: a renovated Maxwell model, J. Nanoparticle Res. 5 (2003) 167–171.